Protein dynamics observed by tunable mid-IR quantum cascade lasers across the time range from 10 ns to 1 s

Bernd-Joachim Schultz[1], Hendrik Mohrmann[1], Victor A. Lorenz-Fonfria[1,2,3] and Joachim Heberle[1*]

[1]Experimental Molecular Biophysics, Department of Physics, Freie Universität Berlin, Arnimallee 14, 14195 Berlin, Germany. [2]Department of Biochemistry and Molecular Biology, Universitat de València, Dr. Moliner 50, 46100 Burjassot, Spain. [3]Interdisciplinary Research Structure for Biotechnology and Biomedicine (ERI BIOTECMED), Universitat de València, Dr. Moliner 50, 46100 Burjassot, Spain.

[*]joachim.heberle@fu-berlin.de

Abstract

We have developed a spectrometer based on tunable quantum cascade lasers (QCLs) for recording time-resolved absorption spectra of proteins in the mid-infrared range. We illustrate its performance by recording time-resolved difference spectra of bacteriorhodopsin in the carboxylic range (1800-1700 cm^{-1}) and on the CO rebinding reaction of myoglobin (1960-1840 cm^{-1}), at a spectral resolution of 1 cm^{-1}. The spectrometric setup covers the time range from 4 ns to nearly a second with a response time of 10-15 ns. Absorption changes as low as 1×10^{-4} are detected in single-shot experiments at $t > 1$ μs, and of 5×10^{-6} in kinetics obtained after averaging 100 shots. While previous time-resolved IR experiments have mostly been conducted on hydrated films of proteins, we demonstrate here that the brilliance of tunable quantum cascade lasers is superior to perform ns time-resolved experiments even in aqueous solution (H_2O).

1. Introduction

Infrared spectroscopy is a powerful tool to record the vibrational spectra of macromolecules. Applying difference spectroscopy, which selects for the vibrational changes to be recorded, changes in single bond vibrations can be registered in front of the background of the absorption of the entire protein. Mid-IR spectroscopy has become a standard tool for determining the secondary structure of proteins, the protonation states of amino acid side chains and the specific interactions of the polypeptide with cofactors and ligands. To trace the sequence of events in the protein´s catalytic action, time-resolved techniques are applied. Different approaches for time-resolved IR spectroscopy have been established in the past decades, which can be classified according to the IR source used: fs-ps pulsed IR lasers, continuous monochromatic IR light emitted from diode lasers, or continuous polychromatic IR emission from a black body radiator.

Flash photolysis techniques in the mid-IR range offer a simple and direct approach to measure reaction kinetics with a time-resolution typically limited by the response time of the IR detector. They rely on continuous monochromatic light sources. Lead salt laser diodes offer output energies of several mW and kinetics are recorded with good signal-to-noise ratio in experiments with nanosecond time resolution [1-3]. However, their mode instabilities and the need for operation at cryogenic temperatures limits their use. A globar as light source, in combination with a monochromator [4, 5], is even lower in output power than lead salt lasers. The tuning range of a monochromator is usually much broader than with any IR laser, although it can be severely reduced by the spectral properties of the monochromator.

Fourier-transform infrared spectroscopy (FT-IR) relies on an interferometer to retrieve spectral information from a polychromatic source such as a globar, eliminating the need for a monochromator. For steady-state absorption experiments, FT-IR spectroscopy is the current gold standard due to its enormously broad spectral range, excellent signal-to-noise ratio and uncontested wavenumber accuracy [6]. Heading for time-resolved experiments, two major FT-based approaches exist. Time-resolved rapid-scan FT-IR [7, 8] records repeatedly interferograms as fast as the

movable mirror completes a moving cycle. Rapid-scan FT-IR provides broadband spectral information and high long-term stability, allowing for reliable time-resolved spectra extending up to tens of seconds [9], or even hours [10]. The time-resolution is 5-10 ms in commercial spectrometers, strongly limiting its applicability to address biological dynamics. Recently, an ultrarapid-scanning FT-IR spectrometer has been presented with 13 microsecond resolution [11].

The step-scan FT-IR technique overcomes the limited time-resolution of rapid-scan at the expense of higher sensitivity to experimental disturbances and longer experimental recordings [12, 13]. In step-scan mode, the movable mirror of the interferometer is fixed at a particular retardation and a kinetic trace is recorded. By consecutively stepping the interferometer mirror to the separate interferogram points one by one and triggering the experimental reaction, a time-resolved interferogram is sampled. These data are re-arranged in such a way to yield interferograms after certain delay times which are Fourier transformed to finally yield time-resolved spectra. Because the interferogram is reconstructed out of independent single recordings, step-scan FT-IR requires highly reversible systems. The total recording time can be very long (hours to days) demanding very stable equipment and samples. Despite these challenges, time-resolved step-scan FT-IR spectroscopy is the reference method for probing the dynamics of photosensitive proteins from nanoseconds to milliseconds [14], arguably the most relevant time scale to protein function.

Since the first experimental implementation of a QCL [15], numerous spectroscopic applications have been realized. Broadly tunable external cavity QCLs became very popular in the recent years. The application of QCLs to the study of proteins aim in two different directions. The majority of applications are heading towards steady-state absorbance measurements which exploit the wavenumber tunability, the high emission power and the highly collimated beam of QCLs: absorbance measurements of proteins in solution [16], slow dynamic changes in the secondary structure of proteins in aqueous solution [17], mapping protein complexes with IR nanoscopy [18] and IR imaging beyond the diffraction limit [19], hyperspectral imaging [20] or vibrational circular dichroism of peptides [21]. The other and less explored direction of QCL applications are kinetic

experiments at high temporal resolution (sub μs), such as in pH-induced protein folding [22, 23], but so far without exploiting the QCL tunability to obtain spectral information. Time-resolved IR difference spectra using tunable QCLs have recently been used to trace structural and protonation changes of the light-gated ion channel channelrhodopsin [24, 25]. However, only few technical details of the experimental setup were reported. Here, the details of the spectrometer are discussed which we developed for recording time-resolved difference spectra of photosensitive systems at high temporal resolution and broad spectral range. We demonstrate that time-resolved spectra of proteins in aqueous solution can be recorded despite the strong background absorption of the solvent water.

The performance of the spectrometer was put to the test for two well-characterized protein systems. Bacteriorhodopsin (bR) is a seven-helical transmembrane protein with all-trans retinal as chromophore. This light-driven proton pump has been the subject of extensive research for decades with the aimed to resolve its functional mechanism [26, 27] as well as to apply new technologies [11]. In particular, bR has been used in pioneering time-resolved IR studies ranging from fs pump-probe experiments [28] to step-scan FTIR with microsecond and nanosecond resolution [29]. As a model metalloprotein, myoglobin (Mb) was employed studying the photo-dissociation of bound carbonmonoxide (CO) [30-32].

2. Design of the spectrometer

Our home-built spectrometer employs tunable quantum cascade lasers as probing light for time-resolved absorption experiments in the mid-infrared region (Fig. 1).

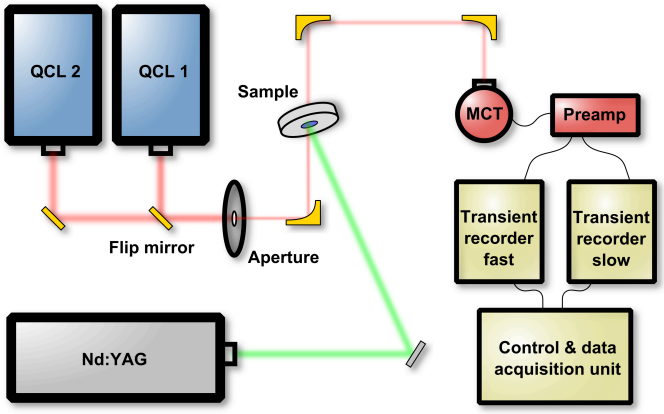

Fig. 1. Setup schematic

Two QCLs (QCL1: model TLS41058; QCL2: TLS41052, Daylight Solutions, San Diego, CA) were used in continuous wave mode. The QCLs provide monochromatic emission of < 0.01 cm^{-1} frequency width. Both lasers were aligned in-plane into the same beam path, and a mirror is flipped to switch between the QCL heads. QCL1 offered a nominal spectral tuning range of 1660 cm^{-1}-1840 cm^{-1}, and QCL2 in the range of 1840 cm^{-1}-1980 cm^{-1}. The output power of the QCLs is about 150 mW at the central frequency of 1740 cm^{-1} for QCL1 and of 1905 cm^{-1} for QCL2. Emission power decreased to both edges of the tuning range before lasing finally ceased accompanied by the rise in intrinsic noise (see 3.2). As a consequence, the signal-to-noise drops when absorbance changes are recorded at the edges of the tuning range. Thus, we limited the analysis of the data to 1700-1800 cm^{-1} for QCL1 and 1880-1960 cm^{-1} for QCL2. The emission power of the QCL can be regulated by the injection current supplied by its controller. We found, however, that the QCL emission estability decreases at lower currents, leading to a QCL-limited noise in the recorded kinetics (hereafter called intrinsic QCL noise). In order to minimize the intrinsic noise, we operated the QCLs at maximum injection current (see 3.3 for more details).

The emitted IR radiation from the QCL was directed to a servo-controlled adjustable aperture (PRM1/MZ8E with SM1D12D, Thorlabs) to prevent saturation of the MCT detector (or even damage of the MCT detector). When the preamplified voltage from the MCT exceeded 1.6 V, the aperture´s diameter was automatically reduced to limit the photon flux. This ensures that the preamplified DC level stays within the digitization range of the oscilloscopes (± 2V) to prevent clipping. After the aperture, the beam was focused on the sample, and afterwards parallelized again by means of two parabolic gold mirrors (f = +4 inch). Depending on the position of the sample with respect to the focal point, the beam diameter at the sample can be varied between 0.1-1 mm. A third off-axis parabolic gold mirror (f = +2 inch) focused the beam onto a photovoltaic MCT detector (KV104-0.5-A3/11, Kolmar Tech Inc.) with a detection element size of 0.5 mm × 0.5 mm and a detectivity of $D^* = 3.25 \times 10^{10}$ cm $Hz^{0.5}$ W^{-1}. An interference filter (Spectrogon bandpass 1200 cm^{-1} to 2000 cm^{-1}) was placed directly in front of the ZnSe detector window to shield the active element of the MCT from stray light from the pulsed visible laser. The MCT was connected to a preamplifier (KA050-A1, Kolmar Tech Inc). The electronic bandwidth of the detector-preamplifier system was 50 MHz. To minimize fluctuations of the detection system, which could contribute as noise in the detected signal, a home-built voltage constanter with a low-noise dual voltage regulator stage was used as power supply. The pre-amplified signal was digitized by two oscilloscopes (Picoscope 4227, Pico Technology) in DC-mode, each with 12 bit vertical resolution, a maximum sampling rate of 250 MS/s, and 32 MSamples of memory (1 MSample = 1,000,000 data points). In the experiments presented here, the fast channel was continuously sampled at a rate of 250 MS/s, and, in parallel, the slow channel with 1 MS/s with 5×10^5 sampling points each.

Photoexcitation of the protein was achieved by a short visible laser pulse. The second harmonic of a quality switched neodymium doped yttrium aluminium garnet laser (Nd:YAG, Minilite II, Continuum) was used which emits a ~6 ns pulse at 532 nm. Data recording by the two oscilloscopes was triggered by a photodiode (180 MHz bandwith, PDA10A, Thorlabs) exposed to a reflection from the exciting laser pulse. In each measurement, 1,000 pretrigger points were collected by each

oscilloscope prior to data recording. This results in 4 μs pretrigger data for the fast channel and 1024 μs for the slow channel. Absorbance differences (ΔA) were calculated by taking the negative decadic logarithm of the measured voltage V(t) at each sampling point divided by the mean pretrigger average V_0: $\Delta A(t) = -\log_{10}\left(\frac{V(t)}{V_0}\right)$

Consequently, the noise in the absorbance kinetics is proportional to the noise in the measured voltage V(t) kinetics and inversely proportional to the intensity of the averaged pretrigger voltage V_0. The time traces recorded by each oscilloscope were averaged on a quasi-logarithmical basis to 60 points per decade, reducing the total amount of data points provided by each oscilloscope from 5×10^5 to ~250 points and, consequently, decreasing the noise level at increasing time delays (see section 3.4). Experiments at a given emission frequency of the QCL were repeated and averaged to further increase the signal-to-noise ratio. The repetition rate of a particular experiment was adapted to the system under study with an upper limit of 20 Hz set by the maximum repetition rate of the pulsed Nd:YAG laser. Finally, both digitized data sets recorded at different oscilloscope sampling rates were merged to yield a trace from nanoseconds to hundreds of milliseconds.

The spectrometer, including auxiliary units, data transfer from the oscilloscopes to a PC and data calculations, was controlled by a home-made graphical interface program running in LabView. All experiments were carried out under dry air atmosphere to minimize absorption of water vapor and fluctuations in the refractive index caused by convection. The temperature of the sample was kept constant at 21.5 °C.

3. Characterisation of the spectrometric setup

The tunable QCL spectrometer was designed to record transient absorption changes of photosensitive proteins in the mid-IR range. The challenge is the recording of very small changes in the order of 10^{-3} to 10^{-5} over the large time scale from 10 ns to many seconds. In the following, the rise time of the detection system was determined and the various sources of noise have been characterized. In all following recordings, the laser power hitting the MCT was kept constant by adaptive attenuation with the motor-driven aperture (Section 2).

3.1 Rise time of the detection system

MCT detector and pre-amplifier have a nominal bandwith of 50 MHz and, thus, an expected response time of around 20 ns. The actual response time was experimentally determined by recording the ultrafast changes in the IR absorption of silicon when excited with a visible pulsed laser. Upon light absorption, Si is electronically excited in the sub-ps time range, followed by electronic and vibrational relaxation processes back to the initial state. We measured the absorption changes of a Si wafer flashed with a visible laser of 6 ns pulse width. As shown in Fig.2, the kinetics at 1720 cm^{-1} and 1905 cm^{-1} show an increase in absorbance followed by a decay (t_0 time was arbitrary). The rise is limited by the response time of the detection system of the spectrometer.

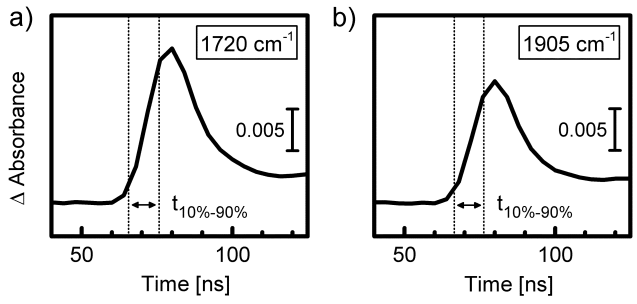

Fig. 2. IR transmission response upon excitation of a Si wafer with a 532 nm laser pulse

a) 1720 cm^{-1} b) 1905 cm^{-1}

The rise time was determined by taking the time for the detector to reach 10-90% of the maximal amplitude which is $t_{10\%-90\%}$ = 10 ns ± 1 ns in both experiments (Fig. 2). We also fitted the data to an exponential decay convoluted with a Gaussian as the instrumental response function (IRF) which yielded a FWHM = 14.9 ns ± 0.2 ns for the IRF.

3.2 Intrinsic noise of the QCL and the dependency on the emission wavelength

In contrast to the (photon-limited) shot noise of visible spectroscopy, noise in FT-IR spectroscopy is detector-limited. Consequently, the noise in the output signal from the detector is independent of the incoming light intensity, and the signal-to-noise ratio scales linearly with the incoming photon flux. The power spectrum of the emission of QCLs is Gaussian shaped. In our QCL spectrometer, the emission power was attenuated to result in a constant photon flux at the MCT detector, irrespective of the selected frequency. We observed, however, that the noise level of different laser heads is different at the same emission frequency despite the same emission power. This observation implies that the noise is not detector-limited in our setup, but limited by fluctuations in the QCL output power (intrinsic QCL noise).

We characterized the intrinsic noise of the QCLs by analyzing single shot kinetics at three different wavenumbers: One at the lower end of the tunability range of the respective QCL (QCL1: 1665 cm^{-1}, QCL2: 1860 cm^{-1}), one at the center frequency (QCL1: 1720 cm^{-1}, QCL2: 1920 cm^{-1}) and one at the higher end (QCL1: 1820 cm^{-1}, QCL2: 1960 cm^{-1}). The respective recordings (Fig. 3) displayed long-term stability of up to 500 ms, independent of the emission wavelength. The RMS of the absorption changes are calculated as a measure of the intrinsic noise of the QCLs (Tab.1).

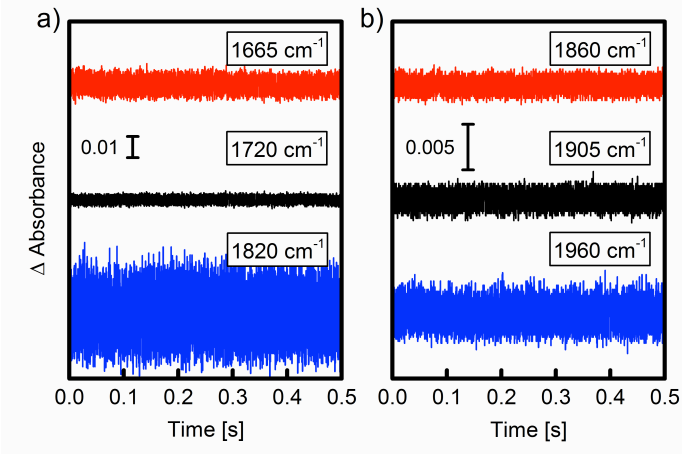

Fig. 3. Single shot kinetics sampled at 1 MS/s at different emission wavenumbers of the QCL at maximum injection current: a) QCL1, b) QCL2

Interestingly, the two QCLs not only exhibit different intrinsic noise levels, but their intrinsic noise also varied at different emission frequencies. While the intrinsic noise of QCL1 rises significantly when tuning the emission frequency towards both edges of the emission spectrum, QCL2 experiences a rise in intrinsic noise only upon tuning towards higher wavenumbers (see Tab.1). Consequently, the performance of the QCLs is poorer towards the edges of the tuning range due to the decreasing output intensity and the increasing intrinsic noise. Thus, the usable tuning ranges is with 1700-1800 cm^{-1} for QCL1 and 1880-1960 cm^{-1} for QCL2 narrower in our experiment than nominal (1660-1840 cm^{-1} for QCL1 and 1840-1980 cm^{-1} for QCL2).

QCL1		*QCL2*	
frequency	*RMS*	*frequency*	*RMS*
1665 cm^{-1}	*1.98×10^{-3}*	*1860 cm^{-1}*	*4.44×10^{-4}*
1720 cm^{-1}	*8.70×10^{-4}*	*1905 cm^{-1}*	*4.62×10^{-4}*
1820 cm^{-1}	*7.04×10^{-3}*	*1960 cm^{-1}*	*8.27×10^{-4}*

Tab. 1. RMS (root-mean-square) deviation of the absorbance at different frequencies for the single shot experiments shown in Fig. 3

3.3 QCL intrinsic noise - injection current dependency

The photon flux of each QCL depends on the injection current in a non-linear manner. To probe the noise of the QCLs at various output photon fluxes, we recorded zero-line single-shot kinetics. The kinetics were taken at the center of the respective tuning range, which is at 1720 cm^{-1} for QCL1 (Fig. 4a) and 1905 cm^{-1} for QCL2 (Fig. 4b).

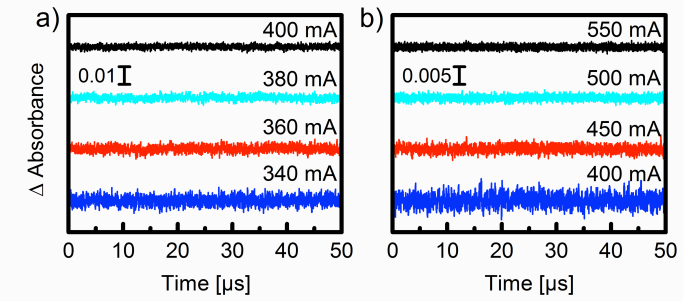

Fig. 4. Kinetic data sampled at 250 MS/s at various injection currents as indicated: a) QCL1 at 1720 cm^{-1}, b) QCL2 at 1905 cm^{-1}. The injection current steps were arbitrarily taken for each QCL.

It is evident from the time traces (Fig. 4) and the RMS (Tab. 2) that the intrinsic noise level increases upon lowering the injection currents. Because the strong emission power of the QCL can saturate or even damage the detector/preamplifier, the QCL beam was attenuated with a motor-driven iris inserted into the beam path, as described in Section 2.

QCL1		*QCL2*	
current	*RMS OD*	*current*	*RMS OD*
400 mA	8.82×10^{-4}	*550 mA*	4.76×10^{-4}
380 mA	1.11×10^{-3}	*500 mA*	5.90×10^{-4}
360 mA	1.52×10^{-3}	*450 mA*	8.27×10^{-4}
340 mA	2.12×10^{-3}	*400 mA*	1.51×10^{-3}

Tab. 2. RMS deviation from the absorbance values at different injection currents

QCL1 at 1720 cm^{-1}, QCL2 at 1905 cm^{-1}

3.4 Performance of the QCL spectrometer

To illustrate the final performance of each QCL under conditions that minimize the intrinsic noise, we recorded zero-line kinetics at emission frequencies that correspond to the center of the tuning range. An increasing number of kinetics were recorded and logarithmically averaged (Fig. 5, Fig. 6).

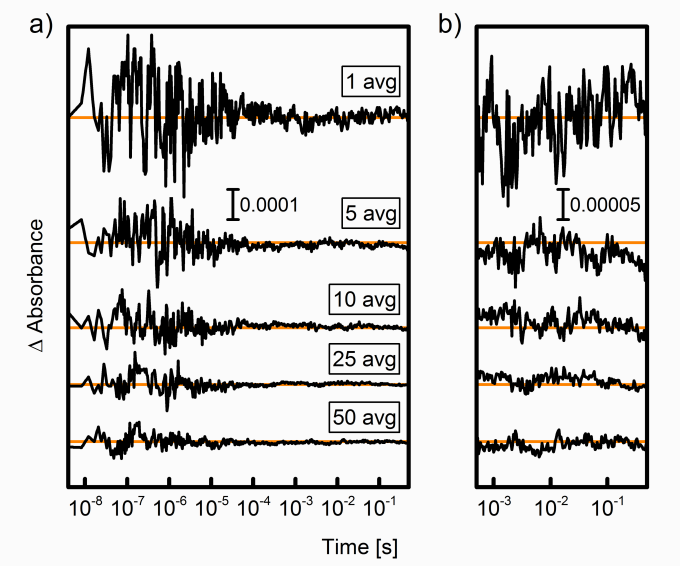

Fig. 5. QCL1 kinetics at 1720 cm^{-1} a) full time scale b) zoomed into the time range of 500 µs - 500 ms (note the different absorbance scale in the two panels)

As can be inferred at best from the single-shot recordings (top traces in Figs.5 and 6), logarithmic averaging reduces the noise level significantly (compare to the time traces in Figs. 3 and 4). From hundreds of microseconds on, the noise level drops by a factor >20. Even in early times, where logarithmic averaging is less efficient, the noise is reduced by a factor >2.

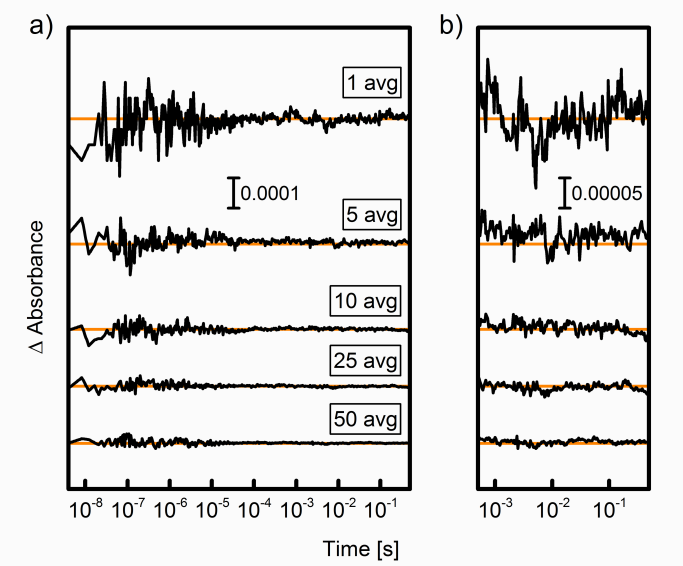

Fig. 6. QCL2 kinetics at 1905 cm^{-1}

a) full time scale b) zoomed in: 500 µs to 500 ms (note the different scale in absorbance)

The RMS of the data for 50 avg in Fig. 5b and Fig. 6b shows $\Delta A < 2\times10^{-5}$ for QCL1 and $< 10^{-5}$ for QCL2. This is the minimum noise level that can be achieved for 50 averages without further data processing.

4. Data post-processing

In a typical time-resolved experiment, time traces are recorded at different frequencies. We exploited the spectral information and the redundancy of the data set to enhance the SNR by spectral smoothing and by singular value decomposition (SVD).

4.1 Spectral smoothing

The QCL spectrometer records kinetics with a discrete wavenumber interval (e.g. each 1 cm^{-1}). We convoluted the raw data in the spectral dimension by a Gaussian. Convolution was done in the Fourier domain by multiplication. The FWHM of the Gaussian determined the resolution of the time-resolved spectra. The results are very similar to FT-IR spectra recorded at the same resolution.

4.2 Singular Value Decomposition

Singular Value Decomposition (SVD) of the collected data, arranged as a matrix, was performed with a home-made routine using the "svd" Matlab function. Denoising is achieved by reconstructing the data using only the significant SVD components. The reconstructed data displays reduced noise but, in contrast to smoothing, does not compromise information provided that a sufficient number of SVD components are used. Further details about SVD can be found in [33, 34]. For the photocycle of bR five intermediates are expected to contribute to the data and, thus, five SVD components should be sufficient to reconstruct the data. Instead we used seven SVD components to ensure data denoising without losing genuine details. For Mb we used two SVD components because the data was simple and straightforward to reconstruct.

5. Application to biological systems

5.1 Materials and method

Rehydrated film samples of bR in the native purple membrane (PM) were prepared as described in [35, 36]. Briefly, ~5 µl of a stock solution of PM (~5 mg/ml in 3 mM KCl and 3 mM potassium phosphate solution, pH 6.5) were deposited on a CaF_2 window and dried to form a film with a diameter of 3 mm. The film was rehydrated by placing nearby a few droplets of a 1:9 glycerol/water mixture (99% relative humidity), and sealed with a second CaF_2 window in a sandwich configuration (Fig. 7a) [37]. For time-resolved step-scan FT-IR experiments, a rehydrated bR film sample was prepared in the same way as mentioned above, except that the sample was spread to form a 8 mm diameter film.

Experiments on samples in solution (H_2O). A total volume of 1 ml solution of 5 mg/ml bR (purple membranes) suspended in 150 mM KCl and 100 mM potassium phosphate buffer, pH 6.5, was centrifuged for 30 min at ~31,500 g. The supernatant was discarded, and the pellet resuspended to 15 mg/ml (~580 µM) as confirmed by UV/Vis spectrosocopy. The sample was placed on a CaF_2 window with a 56 µm thick teflon spacer (Flow Cell, Harrick Scientific), closed with a second window and sealed within the flow cell.

CO-poised myoglobin. The myoglobin (Mb) sample was essentially prepared as described in [30]. The concentration of Mb in solution was ~68 mg/ml (4 mM). For the present experiment, we used a home-made microfluidic device (Fig. 7b). Briefly, a channel of a few micrometer thickness was cut into a thin layer of PDMS (polydimethylsiloxane) and sealed tightly between two CaF_2 windows. The liquid sample was pushed through the channel at continuous flow by the use of a pressure controller (OB1, Elveflow) supplied with Argon gas. The infrared beam and the exciting visible laser beam were focused on the same spot on the channel. While under flow, the sample was excited by the pulsed visible laser and probed by the IR spectrometer. When CO is bound to myoglobin, it is flashed-off by an intense laser pulse (λ = 532 nm, E = 20 mJ/cm^2).

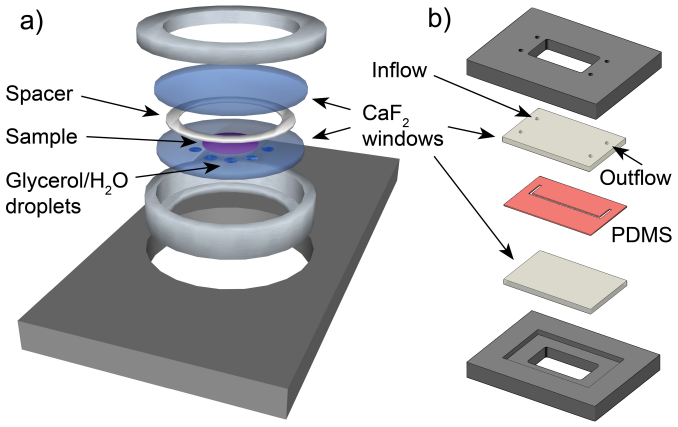

Fig. 7. a) Sandwich cell for rehydrated films and liquid samples

b) PDMS channel for flow-flash experiments of samples in aqueous solution

5.2 Rehydrated bR film

Kinetics of a rehydrated bR film were recorded from 1700 cm^{-1} to 1800 cm^{-1} in steps of 0.5 cm^{-1}. For each measured frequency, the photoreaction was triggered by a short laser flash and recorded 100× at a repetition frequency of 4 Hz, and the resulting kinetic traces were averaged. The sample was hit by 20,100 shots in total, and the whole data recording took ~4 hrs. The data set was treated by SVD, and the first 7 SVD components were used for data reconstruction via linear combination. Global exponential fitting was perfomed on the reconstructed data set. Finally, the data was convoluted by a Gaussian in Fourier space to obtain data with a spectral resolution of 1 cm^{-1}. A 3D representation of the processed time-resolved spectra is shown in Fig. 8. Although the absorption changes are small ($\Delta A \leq 10^{-3}$), the signal-to-noise ratio of the time-resolved data is remarkably high. In this set of experiments, the noise level was as low as 5×10^{-6} at times > 1 µs.

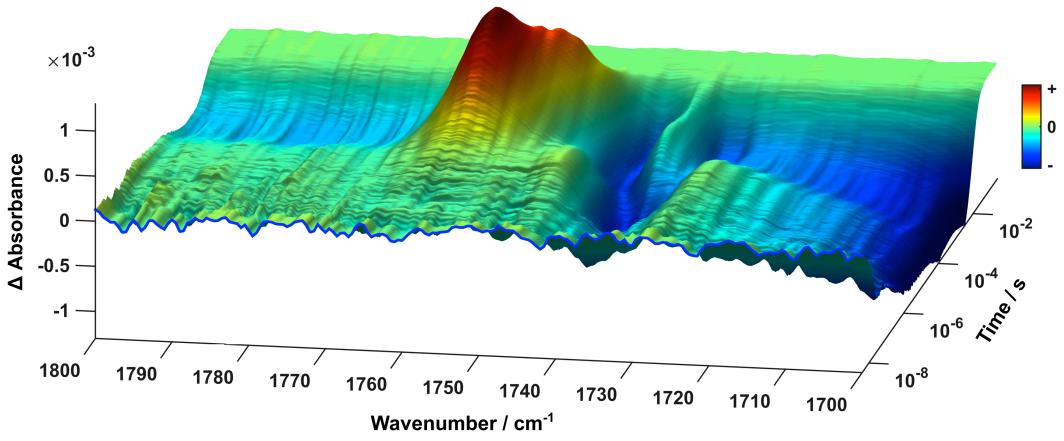

Fig. 8. 3D representation of the absorption changes in the 1800-1700 cm^{-1} spectral range of bR after pulsed laser excitation, as recorded by the QCL spectrometer. The spectra are at 1 cm^{-1} resolution and were reconstructed with 7 SVD components.

For comparison, we performed experiments with time-resolved step-scan FT-IR spectroscopy. Experiments were performed using a commercial spectrometer (Vertex 80v, Bruker Optik, Ettlingen, Germany) at 4 cm^{-1} resolution, measuring photoreactions a 1,332 different optical retardations of the interferogram. The nominal spectral range was from 2,633 cm^{-1} to 0 cm^{-1}, but the useful spectral range was limited to ~2,250 cm^{-1} to 850 cm^{-1} by the optics. For each optical retardation, 32 photoreactions were averaged resulting in a total of ~43,000 repetitions. Due to the instrument response function and the memory capacity of the 24-bit ADC, the time-resolved data was recorded only from 6.25 µs to 50 ms. In constrast, the QCL setup covered a time span from 4 ns to 250 ms . Three relevant time traces at selected frequencies have been extracted from the step-scan data set and overlaid to the QCL data for comparison (Figure 9).

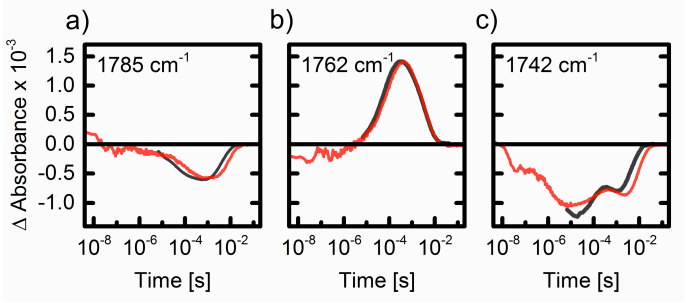

Fig. 9. Time traces for the photocycle of a bR film sample probed at a) 1785 cm^{-1}, b) 1762 cm^{-1}, c) 1742 cm^{-1} (grey: time traces were extracted from step-scan FT-IR spectroscopy and multiplied by ×3.5, 4 cm^{-1} resolution, red: QCL spectrometer, 1 cm^{-1} resolution)

Considering the differences in spectral resolution, the kinetics traces show excellent agreement, irrespective of the light sources used. This observation indicates that the absorption of intense mid-IR emission from the QCL does not lead to a significant increase in temperature in the sample. Otherwise, the kinetics in the QCL experiments would be accelerated because the photoreaction of bR is thermally driven after the initial electronic excitation.

Difference spectra at 100 ns, 2 µs, 300 µs, 10 ms after photoexcitation (Fig. 10a) have been extracted from the data set along with time traces at 1762 cm^{-1} and 1741 cm^{-1} (Fig. 10b,c). Positive differences in this frequency domain correspond to the rise of a C=O stretching vibration assigned to the protonation of carboxylic amino acid side chains. The band at 1762 cm^{-1} in the difference spectrum at 300 µs after the exciting laser pulse (Fig. 7b) reflects protonation of the primary acceptor D85 of the retinal Schiff base (RSB) in the M intermediate of the photocycle of bR [38, 39]. Thus, the rise of the kinetics recorded at 1762 cm^{-1} (Fig. 10b) informs about the time course of proton transfer from the RSB to D85. The decay of the kinetics has two contributions: the shift of the band from 1762 cm^{-1} to 1754 cm^{-1} in the M-to-N intermediate transition, and the deprotonation of D85 in the decay of the O intermediate to the ground state. The spectrum displayed in Fig. 10a, exhibits broad negative absorption at $\nu > 1775$ cm^{-1}. This absorption is characteristic to the continuum band [40] assigned to the release of an excess proton from the internal hydrogen-bonded network of bR [41, 42].

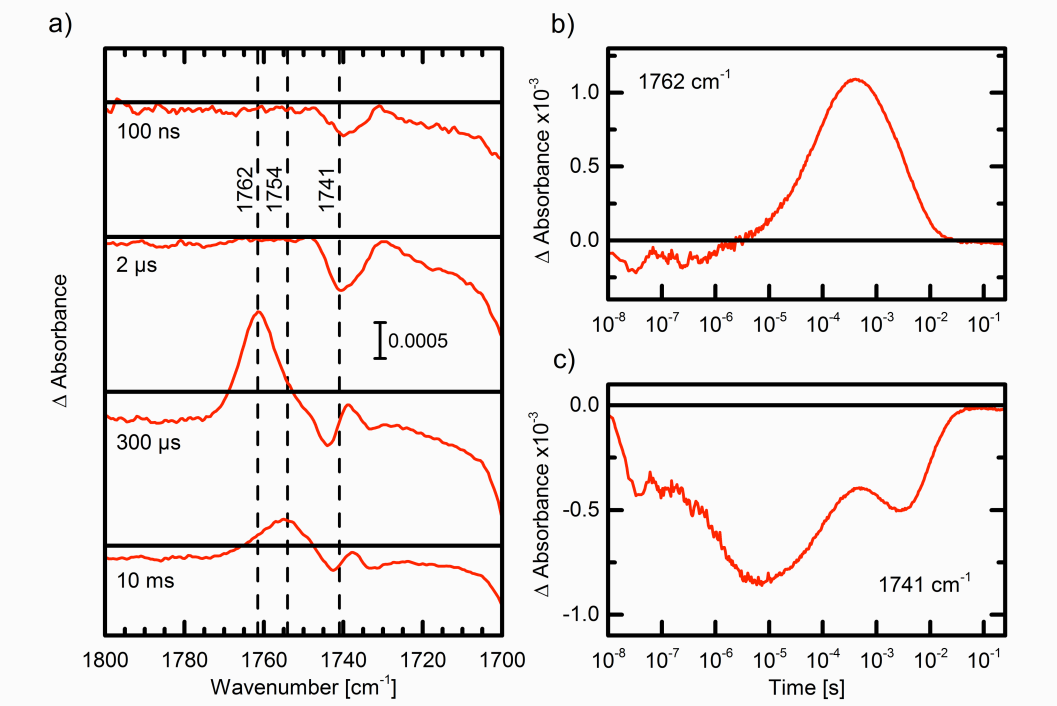

Fig. 10. QCL recordings of a bR film sample at 1 cm^{-1} resolution

a) absorption difference spectra at 100 ns, 2 µs, 300 µs and 10 ms,

b) kinetic trace at 1762 cm^{-1}, c) and at 1741 cm^{-1}.

Fig. 10a displays the difference spectrum recorded at 2 µs after photoexcitation. The negative band at 1741 cm^{-1} has been assigned to hydrogen-bonding changes of the C=O stretching vibrations of the protonated side chains of D96 and D115 [43], which rise upon formation of the L intermediate and decay upon formation of M. D96 transfers its proton to the RSB during the subsequent M-to-N transition. Consequently, the absorption changes at 1741 cm^{-1}, where the C=O stretching vibration of D96 contributes, shows a second negative rise in the early millisecond time range (Fig. 10c). The relative weight of the absorption changes at 1741 cm^{-1} in the micro- and the millisecond time range are pH-dependent and reflect the pK value of D96 in the N intermediate [44].

5.3 Purple membranes suspended in excess water

The high signal-to-noise ratio of the time-resolved data recorded for a hydrated film of PM encouraged us to apply the QCL setup to study the bR photocycle in excess water (PM suspension). The manifold of time-resolved IR spectroscopic published so far have been performed either on hydrated films [45-47], on pellets [29, 48, 49], or on films in contact with excess bulk water [36, 50]. The water content in these samples ranged from 30% to 80% in weight. In the following, we shall present the first time-resolved IR study on bR in its native purple membrane suspended in aqueous solution.

Time-resolved spectra of the bR in solution were recorded from 1700 cm^{-1} to 1800 cm^{-1} in 1 cm^{-1} steps. For each wavenumber probed, the photoreaction was repeated 250 times, resulting in a total of 25,250 recordings collected within about 2.5 hrs (at a repetition rate of 10 Hz).

The kinetics and the spectra resulting from this set of QCL experiments (Fig. 11) agree well with those recorded on the rehydrated bR film sample (Fig. 10). This is particularly valid for the kinetics of the protonation reactions involving the residues D85 and D96.

The noise level in the data on bR in aqueous solution is $< 10^{-5}$. The intrinsic noise of the QCL, which can be clearly seen at early times (Fig. 11 panels b and d), where logarithmic averaging does not effectively kick in, limits the achievable data quality per recorded average. Due to the higher number of averages taken during the experiment with bR in aqueous solution, the corresponding SNR is only slightly less than in the recordings on the hydrated bR film. However, the signals are smaller by almost a factor of ten (Figs. 10 and 11) leading to a reduced SNR.

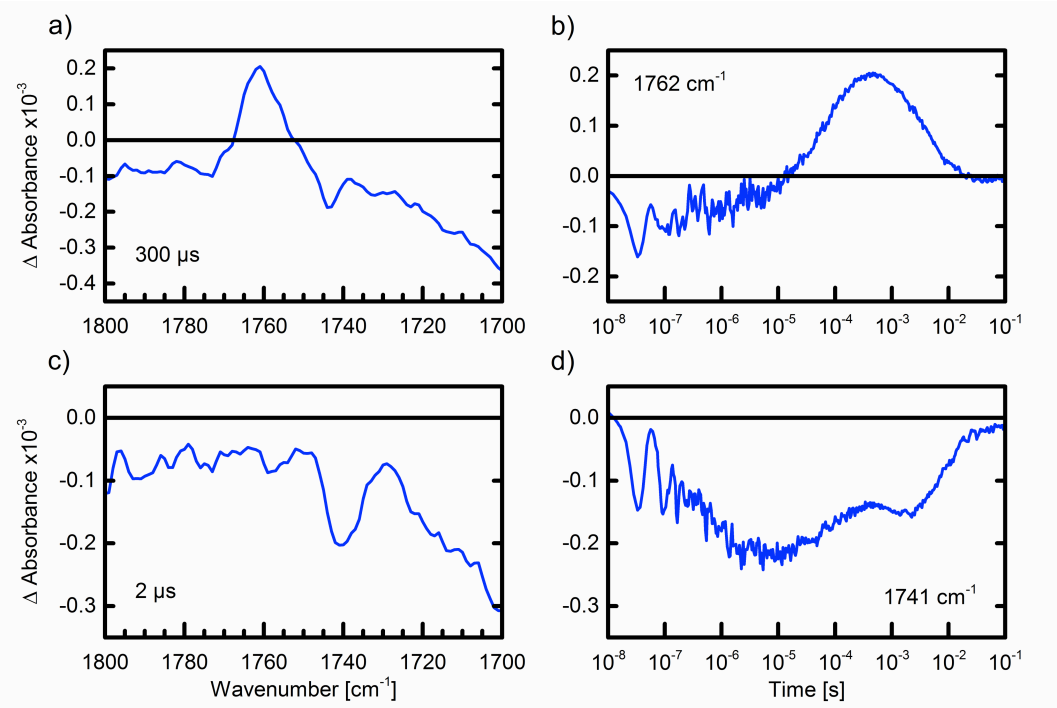

Fig. 11. QCL recordings of bR in aqueous solution at 2 cm^{-1} resolution

a) absorption difference spectrum at 300 µs, b) kinetic trace at 1762 cm^{-1}

c) absorption difference spectrum at 2 µs, d) kinetic trace at 1741 cm^{-1}.

Data have been reconstructed with a linear combination of the 7 most significant SVD components

5.4 Kinetic analysis of the time-resolved IR experiments on bR

Multi-exponential fitting was applied to both data sets of bR yielding 8 time constants for a satisfactory fit to the kinetics of the rehydrated film sample (Tab. 3, column A) and 7 time constants for the sample in solution (Tab. 3 column B).

A	**B**
0.4 [0.3-0.5]	
1.2 [1.0-1.4]	0.8 [0.6-1.0]
8 [6-11]	9 [4-23]
75 [69-82]	76 [62-94]
250 [180-330]	330 [140-780]
2,100[2,000-2,300]	1,700 [1,400-2,000]
6,900 [6,100-7,700]	6,600 [5,700-7,500]
17,000 [6,000-46,000]	37,000 [5,000-300,000]

Tab. 3. Time constants for both bR experiments in µs with the corresponding confidence interval in brackets: **(A)** bR hydrated film, pH 6.5, 294K. QCL (1800-1700 cm^{-1}, 4 ns-250 ms). **(B)** bR solution sample 15 mg/ml, pH 6.5, 294K. QCL (1800-1700 cm^{-1}, 4 ns-100 ms).

The 8 time constants obtained from the QCL recordings of bR in a hydrated film match the time constants derived from ns step-scan FTIR experiments [45],[51] taking into account slight differences in temperature and pH. The step-scan FTIR experiments were recorded over the broader spectral range of 1800-900 cm^{-1} and, thus, richer in information. Despite the fact that the QCL experiments cover a much smaller spectral range (1800-1700 cm^{-1}), the same number of time constants are resolved with time constants of close agreement to those of bR in solution (Tab. 3, columns A and B). Only one time constant, with very small associated amplitude in the spectral range of 1800-1700 cm^{-1}, could not be resolved in solution due to the reduced signal-to-noise ratio.

5.5 MbCO in aqueous solution

Photodissociation of carbonmonoxymyoglobin (Mb-CO) by a short laser pulse yields a short-lived photoproduct, which relaxes to the deoxy-form of myoglobin (deoxy-Mb) [3]. We used CO-poised myglobin (MbCO) as a model system to study heme proteins which are not photoactive under natural conditions. Although the rebinding of photo-dissociated CO to myoglobin is a repetitive reaction, the experiments have been performed under countinuous flow with the sample exchanged after each photo-excitation. This approach simulates experiments on non-repetitive (or very slow-cycling) systems like e.g. the photoreaction of mammalian rhodopsin. The rebinding kinetics of CO to myoglobin is observed only if the flow rate of the protein solution out of the sampling volume is slower.

The C≡O stretching vibration of photodissociated carbonmonoxide appears as a negative difference band at 1943 cm^{-1} in the time-resolved IR difference spectrum (Fig. 12a), indicative of the carbon monoxide ligand bound to reduced heme iron [31]. It is evident that the band is inhomogeneous with additional absorption at the red side of the absorption band. Two Gaussians were fitted to the band and integration yielded a larger band at 1945 cm^{-1} with a relative area of 70% and a smaller band at 1937 cm^{-1} with an area of 30%. According to Li et al. [31] and Makinen et al. [52], these two bands correspond to the A_1 and A_3 conformations of the MbCO.

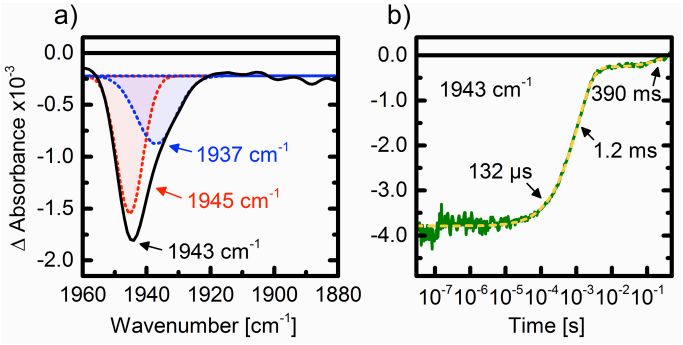

Fig. 12. a) Difference absorbance spectrum of MbCO averaged over 40-60 ns after pulsed photo-dissociation (black trace). The spectrum was reconstructed from single kinetics recorded every 2 cm^{-1} from 1880-1960 cm^{-1}. Each kinetic was recorded for 20 times with a 0.5 Hz repetition rate. This results in a total measurement time of 30 minutes. The data set was treated with SVD and the

first 3 components with highest significance were used for data reconstruction. These data were convoluted in Fourier space by a Gaussian to generate data at a spectral resolution of 4 cm^{-1}. The fit to the sum of two Gaussians (red and blue dotted traces) reproduced the experimental spectrum with the center frequencies of 1945 cm^{-1} and 1937 cm^{-1}.

b) Kinetic of CO rebinding to Mb recorded at 1943 cm^{-1} (green trace). The fit to the sum of three exponentials (dashed orange trace) resulted in time constants of τ_1 = 132 μs, τ_2 = 1.2 ms, and τ_3 = 390 ms.

The kinetics at 1943 cm^{-1} is shown in Fig. 12b. On the basis of the spectrometer response time, the appearance of this negative band is instantaneous. The kinetic trace at 1943 cm^{-1} was fitted to the sum of three exponentials. The rebinding of CO to Mb to form MbCO follows a (pseudo) first order reaction with two time constatnts of τ_1 = 132 μs and τ_2 = 1.2 ms which is close to those derived by Schleeger et al. [30]. A third time constant, of τ_3 = 390 ms, corresponds to the process of exchange of the sample volume in the microfluidic cell under the pressure applied to push the sample forward. For a channel thickness of 50 μm in our experiment, we calculate a complete sample exchange out of the IR measuring beam spot of ~300 ms. This is in the order of our recorded results.

This experiment shows two distinct advantages of the QCL setup over step-scan FT-IR spectroscopy. Due to the high power of the QCL, sample cells with longer optical pathlength can be used which would lead to the absorption of almost all light emitted by the weak source of a blackbody radiator of an FTIR photometer. In the QCL experiments, we used a sample pathlength of ~50 μm which can be even larger which resulted in strong difference bands in the time-resolved experiments. As a consequence, only 10 averages at a repetition rate of 0.5 Hz were sufficient to yield kinetics with high S/N-ratio as displayed in Fig. 12b. The latter data was taken within 25 seconds which compares to more than 1 hour for a step scan FT-IR experiment recorded under otherwise identical conditions [30]. However, this comparison is only valid if spectral information

on particular marker bands has already been retrived. In this case, lower sample consumption is an issue for precious samples like membrane proteins that are difficult to prepare.

6. Conclusions

We have developed a spectrometer based on tunable QCLs for recording time-resolved difference spectra in the mid-IR range. The recorded data from the model systems bR and MbCO agree well with published time-resolved FT-IR spectroscopy experiments using the step-scan technique [29, 30, 53]. The major advantage of our QCL setup is the straightforward measurement of strong absorbing samples which relates to the high emission power of QCLs. Compared to the maximum emission power of ~15 $\mu W/cm^{-1}$ of a globar under standard operational conditions, a QCL emits much higher radiation powers of 50-400 mW/cm^{-1}. MCT detectors that are typically used for mid-IR spectroscopy, are not limited by shot noise. Thus, more intense radiation will lead to less noise. The use of QCLs as light sources makes it possible to measure larger pathlengths and, therefore, obtain larger difference signals from the sample. Even when recording only a few averages, the noise in the absorption change drops to levels as low as 10^{-5}. The QCL, however, remains the critical part of the experimental setup. Depending on the intrinsic noise of the individual head and the selected output frequency, the number of averages required to yield low noise data can raise substantially.

Another unique feature of our QCL setup is the possibility to record the kinetics of slow-cycling systems or even irreversible reactions. This situation is usually very challenging to step-scan FT-IR spectroscopy as the technique requires many repetitions of a strictly reversible process. We have already applied the spectrometer to slow-cycling systems, such as the light-gated ion channel channelrhodopsin-2 [24, 25], including experiments in the amide I range (1600-1700 cm^{-1} using a different QCL head). The application of a flowcell opens an avenue to measure non-cyclic systems, like e.g. visual rhodopsin, or chemical and enzymatic transformations in aqueous solutions (H_2O).

The narrow bandwidth of the QCL emisson (< 0.01 cm^{-1}) offers the possibility of time-resolved spectroscopy at high spectral resolution. Indeed, we have presented here time-resolved IR difference spectra of bR in the carboxylic region at a spectral resolution of 1 cm^{-1} which is superior to time-resolved step-scan FTIR spectroscopy where spectra have been recorded with the highest spectral resolution of 3.5 cm^{-1} reported for proteins [29] .

Finally, step-scan FT-IR spectroscopy has the undisputed merit of providing a broadband spectral information in the mid-IR region ($\Delta\nu \approx$ 3000-1000 cm^{-1}), while each EC-QCL head exhibits a (useful) tunability range of 100-150 cm^{-1}. Still, both approaches can be considered complementary. Once a marker band has been identified by either static or time-resolved FT-IR spectroscopy, our novel QCL spectrometer will allow to measure in few seconds the kinetics with with a time resolution of 10 ns. Moreover, QCLs emit collimated radiation which is much easier to focus than the emission of a globar. Thus, spectroscopy on micrometer sized objects like protein crystals used for femtosecond serial crystallography [54] are facilitated in order to correlate time-resolved structural and spectroscopic experiments. Time-resolved IR experiments on the nanometer scale are also envisaged when near-field effects at an AFM tip are exploited [18].

Acknowledgements.

Funding was provided by the German Research Foundation through SFB-1078, projects A1 and B3 to J.H. V.A.L.-F. is a Ramón y Cajal Fellow (RYC-2013-13114, Ministerio de Economía y Competitividad). We acknowledge support by the focus area Nanoscale of the Freie Universität Berlin. We thank Dorothea Heinrich and Jessica Stapel for sample preparation.

References

[1] D.T. Leeson, F. Gai, H.M. Rodriguez, L.M. Gregoret, R.B. Dyer, Protein folding and unfolding on a complex energy landscape, Proc Natl Acad Sci U S A, 97 (2000) 2527-2532.
[2] J. Lin, K. Gerwert, C. Kotting, A modified infrared spectrometer with high time resolution and its application for investigating fast conformational changes of the GTPase Ras, Appl Spectrosc, 68 (2014) 531-535.
[3] T.P. Causgrove, R.B. Dyer, Protein response to photodissociation of CO from carbonmonoxymyoglobin probed by time-resolved infrared spectroscopy of the amide I band, Biochemistry, 32 (1993) 11985-11991.
[4] F. Siebert, W. Mäntele, W. Kreutz, Flash-induced kinetic infrared spectroscopy applied to biochemical systems, Biophys Struct Mech, 6 (1980) 139-146.
[5] J. Sasaki, A. Maeda, C. Kato, H. Hamaguchi, Time-resolved infrared spectral analysis of the KL-to-L conversion in the photocycle of bacteriorhodopsin, Biochemistry, 32 (1993) 867-871.
[6] F. Siebert, P. Hildebrandt, Vibrational Spectroscopy in Life Science, Wiley-VCH, 2007.
[7] K. Gerwert, G. Souvignier, B. Hess, Simultaneous monitoring of light-induced changes in protein side-group protonation by time resolved Fourier-transform infrared spectroscopy, Proc.Natl.Acad.Sci.USA, 87 (1990) 9774-9778.
[8] I. Radu, M. Schleeger, C. Bolwien, J. Heberle, Time-resolved methods in biophysics. 10. Time-resolved FT-IR difference spectroscopy and the application to membrane proteins, Photochem Photobiol Sci, 8 (2009) 1517-1528.
[9] V.A. Lórenz-Fonfría, V. Muders, R. Schlesinger, J. Heberle, Changes in the hydrogen-bonding strength of internal water molecules and cysteine residues in the conductive state of channelrhodopsin-1, J Chem Phys, 141 (2014) 22D507.
[10] N. Dave, V.A. Lórenz-Fonfría, J. Villaverde, R. Lemonnier, G. Leblanc, E. Padros, Study of amide-proton exchange of Escherichia coli melibiose permease by attenuated total reflection-Fourier transform infrared spectroscopy: evidence of structure modulation by substrate binding, J Biol Chem, 277 (2002) 3380-3387.
[11] B. Süss, F. Ringleb, J. Heberle, New ultrarapid-scanning interferometer for FT-IR spectroscopy with microsecond time-resolution, Rev Sci Instrum, 87 (2016) 063113.
[12] W. Uhmann, A. Becker, C. Taran, F. Siebert, Time-Resolved Ft-Ir Absorption-Spectroscopy Using a Step-Scan Interferometer, Appl Spectrosc, 45 (1991) 390-397.
[13] G.D. Smith, R.A. Palmer, Fast Time-Resolved Mid-Infrared Spectroscopy Using an Interferometer, in: Handbook of Vibrational Spectroscopy, John Wiley & Sons, Ltd, 2006.
[14] K. Gerwert, Molecular Reaction Mechanisms of Proteins Monitored by Time-Resolved FT-IR Difference Spectroscopy, in: Handbook of Vibrational Spectroscopy, John Wiley & Sons, Ltd, 2006.
[15] J. Faist, F. Capasso, D.L. Sivco, C. Sirtori, A.L. Hutchinson, A.Y. Cho, Quantum cascade laser, Science, 264 (1994) 553-556.
[16] M.R. Alcaraz, A. Schwaighofer, C. Kristament, G. Ramer, M. Brandstetter, H. Goicoechea, B. Lendl, External-Cavity Quantum Cascade Laser Spectroscopy for Mid-IR Transmission Measurements of Proteins in Aqueous Solution, Anal Chem, 87 (2015) 6980-6987.
[17] M.R. Alcaraz, A. Schwaighofer, H. Goicoechea, B. Lendl, EC-QCL mid-IR transmission spectroscopy for monitoring dynamic changes of protein secondary structure in aqueous solution on the example of beta-aggregation in alcohol-denaturated alpha-chymotrypsin, Anal Bioanal Chem, 408 (2016) 3933-3941.
[18] I. Amenabar, S. Poly, W. Nuansing, E.H. Hubrich, A.A. Govyadinov, F. Huth, R. Krutokhvostov, L. Zhang, M. Knez, J. Heberle, A.M. Bittner, R. Hillenbrand, Structural analysis and mapping of individual protein complexes by infrared nanospectroscopy, Nat Commun, 4 (2013) 2890.
[19] A. Centrone, Infrared Imaging and Spectroscopy Beyond the Diffraction Limit, Annu Rev Anal Chem (Palo Alto Calif), 8 (2015) 101-126.
[20] A. Goyal, T. Myers, C.A. Wang, M. Kelly, B. Tyrrell, B. Gokden, A. Sanchez, G. Turner, F. Capasso, Active hyperspectral imaging using a quantum cascade laser (QCL) array and digital-pixel focal plane array (DFPA) camera, Opt Express, 22 (2014) 14392-14401.
[21] A. Ruther, M. Pfeifer, V.A. Lórenz-Fonfría, S. Ludeke, pH titration monitored by quantum cascade laser-based vibrational circular dichroism, J Phys Chem B, 118 (2014) 3941-3949.
[22] M.L. Donten, S. Hassan, A. Popp, J. Halter, K. Hauser, P. Hamm, pH-jump induced leucine zipper folding beyond the diffusion limit, J Phys Chem B, 119 (2015) 1425-1432.
[23] B.L. Greene, C.H. Wu, P.M. McTernan, M.W.W. Adams, R.B. Dyer, Proton-Coupled Electron Transfer Dynamics in the Catalytic Mechanism of a [NiFe]-Hydrogenase, J Am Chem Soc, 137 (2015) 4558-4566.
[24] T. Resler, B.J. Schultz, V.A. Lórenz-Fonfría, R. Schlesinger, J. Heberle, Kinetic and vibrational isotope effects of proton transfer reactions in channelrhodopsin-2, Biophys J, 109 (2015) 287-297.
[25] V.A. Lórenz-Fonfría, B.J. Schultz, T. Resler, R. Schlesinger, C. Bamann, E. Bamberg, J. Heberle, Pre-gating conformational changes in the ChETA variant of channelrhodopsin-2 monitored by nanosecond IR spectroscopy, J Am Chem Soc, 137 (2015) 1850-1861.
[26] J. Heberle, J. Fitter, H.J. Sass, G. Buldt, Bacteriorhodopsin: the functional details of a molecular machine are being resolved, Biophys Chem, 85 (2000) 229-248.

[27] C. Zscherp, J. Heberle, Infrared difference spectra of the intermediates L, M, N, and O of the bacteriorhodopsin photoreaction obtained by time-resolved attenuated total reflection spectroscopy, J Phys Chem B, 101 (1997) 10542-10547.
[28] J. Herbst, K. Heyne, R. Diller, Femtosecond infrared spectroscopy of bacteriorhodopsin chromophore isomerization, Science, 297 (2002) 822-825.
[29] R. Rammelsberg, B. Hessling, H. Chorongiewski, K. Gerwert, Molecular reaction mechanisms of proteins monitored by nanosecond step-scan FT-IR difference spectroscopy, Appl Spectrosc, 51 (1997) 558-562.
[30] M. Schleeger, C. Wagner, M.J. Vellekoop, B. Lendl, J. Heberle, Time-resolved flow-flash FT-IR difference spectroscopy: the kinetics of CO photodissociation from myoglobin revisited, Anal Bioanal Chem, 394 (2009) 1869-1877.
[31] T. Li, M.L. Quillin, G.N. Phillips, Jr., J.S. Olson, Structural determinants of the stretching frequency of CO bound to myoglobin, Biochemistry, 33 (1994) 1433-1446.
[32] T.R. Barends, L. Foucar, A. Ardevol, K. Nass, A. Aquila, S. Botha, R.B. Doak, K. Falahati, E. Hartmann, M. Hilpert, M. Heinz, M.C. Hoffmann, J. Kofinger, J.E. Koglin, G. Kovacsova, M. Liang, D. Milathianaki, H.T. Lemke, J. Reinstein, C.M. Roome, R.L. Shoeman, G.J. Williams, I. Burghardt, G. Hummer, S. Boutet, I. Schlichting, Direct observation of ultrafast collective motions in CO myoglobin upon ligand dissociation, Science, 350 (2015) 445-450.
[33] V.A. Lórenz-Fonfría, H. Kandori, Spectroscopic and kinetic evidence on how bacteriorhodopsin accomplishes vectorial proton transport under functional conditions, J Am Chem Soc, 131 (2009) 5891-5901.
[34] R.W. Hendler, R.I. Shrager, Deconvolutions based on singular value decomposition and the pseudoinverse: a guide for beginners, J Biochem Biophys Methods, 28 (1994) 1-33.
[35] V.A. Lórenz-Fonfría, T. Resler, N. Krause, M. Nack, M. Gossing, G. Fischer von Mollard, C. Bamann, E. Bamberg, R. Schlesinger, J. Heberle, Transient protonation changes in channelrhodopsin-2 and their relevance to channel gating, Proc Natl Acad Sci U S A, 110 (2013) E1273-1281.
[36] V.A. Lórenz-Fonfría, J. Heberle, Proton transfer and protein conformation dynamics in photosensitive proteins by time-resolved step-scan Fourier-transform infrared spectroscopy, J Vis Exp, (2014) e51622.
[37] T. Noguchi, M. Sugiura, Flash-induced FTIR difference spectra of the water oxidizing complex in moderately hydrated photosystem II core films: effect of hydration extent on S-state transitions, Biochemistry, 41 (2002) 2322-2330.
[38] K. Fahmy, O. Weidlich, M. Engelhard, J. Tittor, D. Oesterhelt, F. Siebert, Identification of the proton acceptor of Schiff-base deprotonation in bacteriorhodopsin - a Fourier-transform infrared study of the mutant Asp85-Glu in its natural lipid environment, Photochem. Photobiol., 56 (1992) 1073-1083.
[39] M.S. Braiman, T. Mogi, T. Marti, L.J. Stern, H.G. Khorana, K.J. Rothschild, Vibrational spectroscopy of bacteriorhodopsin mutants: light-driven proton transport involves protonation changes of aspartic acid residues 85, 96, and 212, Biochemistry, 27 (1988) 8516-8520.
[40] J. Le Coutre, J. Tittor, D. Oesterhelt, K. Gerwert, Experimental evidence for hydrogen-bonded network proton transfer in bacteriorhodopsin shown by Fourier-transform infrared spectroscopy using azide as catalyst, Proc Natl Acad Sci U S A, 92 (1995) 4962-4966.
[41] F. Garczarek, J. Wang, M.A. El-Sayed, K. Gerwert, The assignment of the different infrared continuum absorbance changes observed in the 3000-1800-cm(-1) region during the bacteriorhodopsin photocycle, Biophys J, 87 (2004) 2676-2682.
[42] J. Heberle, A local area network of protonated water molecules, Biophys J, 87 (2004) 2105-2106.
[43] J. Sasaki, J.K. Lanyi, R. Needleman, T. Yoshizawa, A. Maeda, Complete identification of C = O stretching vibrational bands of protonated aspartic acid residues in the difference infrared spectra of M and N intermediates versus bacteriorhodopsin, Biochemistry, 33 (1994) 3178-3184.
[44] C. Zscherp, R. Schlesinger, J. Tittor, D. Oesterhelt, J. Heberle, In situ determination of transient pK(a) changes of internal amino acids of bacteriorhodopsin by using time-resolved attenuated total reflection Fourier-transform infrared spectroscopy, Proc Natl Acad Sci USA, 96 (1999) 5498-5503.
[45] C. Rodig, I. Chizhov, O. Weidlich, F. Siebert, Time-resolved step-scan Fourier transform infrared spectroscopy reveals differences between early and late M intermediates of bacteriorhodopsin, Biophys J, 76 (1999) 2687-2701.
[46] V.A. Lórenz-Fonfría, Y. Furutani, H. Kandori, Active internal waters in the bacteriorhodopsin photocycle. A comparative study of the L and M intermediates at room and cryogenic temperatures by infrared spectroscopy, Biochemistry, 47 (2008) 4071-4081.
[47] R. Diller, M. Iannone, R. Bogomolni, R.M. Hochstrasser, Ultrafast infrared spectroscopy of bacteriorhodopsin, Biophys J, 60 (1991) 286-289.
[48] A.K. Dioumaev, M.S. Braiman, Two bathointermediates of the bacteriorhodopsin photocycle, distinguished by nanosecond time-resolved FTIR spectroscopy at room temperature, J Phys Chem B, 101 (1997) 1655-1662.
[49] W. Hage, M. Kim, H. Frei, R.A. Mathies, Protein dynamics in the bacteriorhodopsin photocycle: A nanosecond step-scan FTIR investigation of the KL to L transition, J Phys Chem, 100 (1996) 16026-16033.
[50] J. Heberle, C. Zscherp, ATR/FT-IR difference spectroscopy of biological matter with microsecond time resolution, Appl Spectrosc, 50 (1996) 588-596.
[51] R. Rammelsberg, G. Huhn, M. Lubben, K. Gerwert, Bacteriorhodopsin's intramolecular proton-release pathway consists of a hydrogen-bonded network, Biochemistry, 37 (1998) 5001-5009.

[52] M.W. Makinen, R.A. Houtchens, W.S. Caughey, Structure of carboxymyoglobin in crystals and in solution, Proc Natl Acad Sci U S A, 76 (1979) 6042-6046.
[53] V.A. Lórenz-Fonfría, H. Kandori, E. Padros, Probing specific molecular processes and intermediates by time-resolved Fourier transform infrared spectroscopy: application to the bacteriorhodopsin photocycle, J Phys Chem B, 115 (2011) 7972-7985.
[54] A. Aquila, M.S. Hunter, R.B. Doak, R.A. Kirian, P. Fromme, T.A. White, J. Andreasson, D. Arnlund, S. Bajt, T.R. Barends, M. Barthelmess, M.J. Bogan, C. Bostedt, H. Bottin, J.D. Bozek, C. Caleman, N. Coppola, J. Davidsson, D.P. DePonte, V. Elser, S.W. Epp, B. Erk, H. Fleckenstein, L. Foucar, M. Frank, R. Fromme, H. Graafsma, I. Grotjohann, L. Gumprecht, J. Hajdu, C.Y. Hampton, A. Hartmann, R. Hartmann, S. Hau-Riege, G. Hauser, H. Hirsemann, P. Holl, J.M. Holton, A. Homke, L. Johansson, N. Kimmel, S. Kassemeyer, F. Krasniqi, K.U. Kuhnel, M. Liang, L. Lomb, E. Malmerberg, S. Marchesini, A.V. Martin, F.R. Maia, M. Messerschmidt, K. Nass, C. Reich, R. Neutze, D. Rolles, B. Rudek, A. Rudenko, I. Schlichting, C. Schmidt, K.E. Schmidt, J. Schulz, M.M. Seibert, R.L. Shoeman, R. Sierra, H. Soltau, D. Starodub, F. Stellato, S. Stern, L. Struder, N. Timneanu, J. Ullrich, X. Wang, G.J. Williams, G. Weidenspointner, U. Weierstall, C. Wunderer, A. Barty, J.C. Spence, H.N. Chapman, Time-resolved protein nanocrystallography using an X-ray free-electron laser, Opt Express, 20 (2012) 2706-2716.